

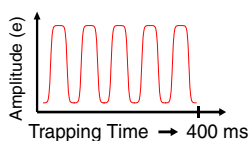
## RESEARCH ARTICLE

# Charge Detection Mass Spectrometry for Single Ions with an Uncertainty in the Charge Measurement of 0.65 e

Elizabeth E. Pierson, Nathan C. Contino, David Z. Keifer, Martin F. Jarrold

Chemistry Department, Indiana University, 800 E. Kirkwood Avenue, Bloomington, IN 47405, USA

## Charge Detection Mass Spectrometry



Charge Accuracy = 0.65e

**Abstract.** Charge detection mass spectrometry (CDMS) provides a direct measure of the mass of individual ions through nondestructive, simultaneous measurements of the mass to charge ratio and the charge. To improve the accuracy of the charge measurement, ions are trapped and recirculated through the charge detector. By substantially extending the trapping time, the uncertainty in the charge determination has been reduced by a factor of two, from 1.3 elementary charges (e) to 0.65 e. The limit of detection (the smallest charge that can be reliably measured) has been reduced by about the same proportion, from 13 to 7 e. The more precise charge measurements enable a substantial improvement in the mass resolution, which is critical for applications of CDMS to mixtures of high mass ions.

**Keywords:** Charge detection mass spectrometry

Received: 17 February 2015/Revised: 2 March 2015/Accepted: 4 March 2015/Published Online: 14 April 2015

## Introduction

Charge detection mass spectrometry (CDMS) is a technique in which simultaneous measurement of the mass-to-charge ratio ( $m/z$ ) and the charge ( $z$ ) of individual ions yields the mass of each ion. This approach circumvents the need to resolve charge states in a traditional  $m/z$  spectrum from an electrospray source, which can become convoluted for ions above several hundred kDa [1, 2]. To measure  $m/z$  and  $z$ , an ion with a known kinetic energy is passed through a conducting cylinder and the charge induced on the cylinder is detected. The length of the signal (the time-of-flight through the tube) is related to the ion's  $m/z$ . The amplitude of the signal is proportional to  $z$ . Multiplying  $m/z$  and  $z$  for each ion yields  $m$ ; the  $m$  values are then binned to generate a mass spectrum.

Simultaneous detection of  $m/z$  and  $z$  was first used by Shelton and co-workers more than 50 years ago to determine the mass of highly-charged, micron-sized particles [3]. The smallest particle detected was 0.2  $\mu\text{m}$  in diameter with nearly 20,000 elementary charges (e). Hendricks later published a study using a similar detector to size oil droplets generated by electrohydrodynamic spraying [4]. He found that the charged oil droplets were near the Rayleigh limit [5]. In 1990, Keaton et al. and Stradling et al. developed a more sensitive apparatus of the Shelton design with a limit of detection of  $\sim 1500$  charges [6, 7].

The growing interest in mass spectrometry of noncovalent protein complexes and nucleic acids in the early 1990s prompted the Smith group to develop a Fourier transform ion cyclotron resonance (FTICR) approach that was able to trap single, MDa-size DNA ions and simultaneously measure their  $m/z$  and  $z$  [8]. In this approach, charges states as low as +30 were detected with a precision of  $\pm 10\%$ . Despite this success, the expensive instrumentation and the low accuracy associated with the charge measurement has limited its use.

As an alternative to FTICR for measuring the mass of MDa-size particles, Fuerstenau and Benner and coworkers coupled an electrospray source with CDMS to measure the mass of DNA and polystyrene microspheres [9–11]. The detector used in these studies was modeled after the original Shelton design. The energy distribution of electrospray ions in this experiment was broad and precluded proper  $m/z$  determination. Instead, Benner measured the velocity of particles from the expansion into vacuum (with all electrodes grounded) and the velocity of particles after acceleration across a known potential. The velocity difference allowed  $m/z$  determination. The precision of the charge measurement was  $\pm 75$  e, and the limit of detection was  $\sim 330$  e. A few years later, Fuerstenau and Benner's single-pass method [12, 13] was used to measure the masses of whole viruses, although the mass resolution achieved in these early experiments was limited by the precision of the charge measurement.

Recently, some groups have used CDMS in a variety of high-mass applications that have not required precise charge measurements. Antoine, Dugourd, and collaborators studied

the charging capacity of poly(ethylene oxide) (PEO) ions with masses of up to 7 MDa [14]. Based on the lower-than-expected charging, they concluded that PEO was not fully extended in the gas phase. The same group used CDMS to study the photodissociation of single PEO ions [15] and the size distribution of self-assembled amphiphilic block co-polymers [16]. In related work, Chang and collaborators used the basic principle of concurrent  $z$  and  $m/z$  determination to measure the mass of red blood cells [17].

One way to improve the precision of the charge measurement is to signal average. To this end, Benner situated his charge detector within an electrostatic ion trap to perform multiple  $m/z$  and  $z$  measurements for each ion [18]. The error in the charge measurement is expected to decrease by a factor of  $n^{1/2}$  where  $n$  is the number of cycles an ion is trapped. In that work, ions were trapped for up to 450 cycles. With a root mean square (RMS) noise of 50 e, the charge measurements could theoretically be as precise as  $\pm 2.4$  e. However, the limit of detection was still high ( $\sim 250$  e). An alternative approach to multiple charge measurements, first implemented by Gamero-Castaño is the use of a linear array of charge detectors [19–22]. However, although offering the advantage of higher throughput, it has not been possible to achieve the charge accuracy obtained with a recirculating trap.

Recent work in our group has focused on lowering the limits of detection and improving the accuracy and precision of the measurements made with a CDMS ion trap [23, 24]. The first CDMS instrument used in our lab contained a single-pass charge detector with a limit of detection of  $\sim 1000$  e and a charge error of 15%. This set-up was used to study the aerodynamic breakup of water droplets in the electrospray vacuum interface [25] and droplet breakup in vacuum due to freezing [26]. In our current CDMS instrument, the charge detector lies at the center of an electrostatic ion trap. The endcaps of the trap are conical and it is modeled after the design of Schmidt et al. [27]. The trap is preceded by a dual hemispherical deflection analyzer (HDA) [28, 29], which transmits a narrow band of ion kinetic energies. We first reported the mass of bovine serum albumin ions trapped for up to 29 ms [23]. The lower limit of detection was 30 e and simulations indicated that the uncertainty in charge was 3.2 e. A key improvement was made by cryogenically cooling the junction field-effect transistor (JFET) located at the input of the charge-sensitive preamplifier that senses the induced charge. Cooling the JFET increases the transconductance and lowers the thermal noise. As a result, the S/N was increased by a factor of 1.7, which improved both the accuracy of the charge measurement and the limit of detection [24]. With this improvement we were able to resolve charge states in the  $m/z$  spectrum using CDMS. This allowed a direct comparison of the charge determined from the  $m/z$  spectrum with the charge determined from the charge measurement. For the first time, the accuracy of the charge measurement could be evaluated directly. The RMS deviation of the charge measurement was determined to be 2.2 e for alcohol dehydrogenase ions trapped for up to 29 ms (around 1500 cycles). In addition, because of the improved S/N the limit of

detection (the lowest charge that could be reliably measured) was lowered to 13 e. Ions with as few as nine charges were detected, but their detection efficiency was low and the measured charge was too high.

The RMS deviation of the charge measurement is expected to be inversely proportional to the square root of the trapping time. By increasing the trapping time to 129 ms, we were able to improve the accuracy of the charge measurements to 1.3 e, though only 1% of the ions were trapped for this long [2]. This configuration has now been used to probe higher order multimers of pyruvate kinase [2], the mass distribution of 24-MDa bacteriophage P22 procapsids [30] late intermediates in the assembly of hepatitis B virus capsids [31] and woodchuck hepatitis virus [32].

In the work presented here, we have made a number of modifications to the experiment so that ions are more efficiently trapped, allowing us to trap ions for much longer. As a result of these modifications, up to 70% of the ions from an electrosprayed pyruvate kinase solution can now be trapped for 391 ms, compared with less than 1% trapped for 129 ms in our previous experiments [2]. This dramatic increase in the trapping time leads to a substantial improvement in the accuracy of the charge measurement. The RMS deviation of the charge measurement has been reduced to 0.65 e. The limit of detection has also been lowered by a factor of two. Charge states as low as +7 have been reliably detected for ubiquitin. The improved accuracy of the charge measurements leads to a marked improvement in the mass resolution achieved with CDMS, which is important in the analysis of mixtures of high mass ions.

## Experimental

The experimental apparatus has been described in detail elsewhere [24, 27], so only a brief description will be provided here. Measurements were performed for ubiquitin, cytochrome *c*, and pyruvate kinase. Ubiquitin and cytochrome *c* ions were generated by electrospray with a pulled tip, desolvated by a countercurrent of warm, dry air, and introduced into the vacuum chamber through a 0.5 mm diameter aperture. For pyruvate kinase, an automated nanoelectrospray source replaces the pulled tip and a stainless steel capillary interface replaces the aperture since this set-up is more amenable for the analysis of large ions. Once in the vacuum chamber, ions pass through three differentially pumped regions before entering the analysis chamber. The first differentially pumped region contains an ion funnel [28] and the next two contain a hexapole and quadrupole, respectively, supplied with rf voltages. The DC offset on the hexapole defines the nominal ion energy. This is set at 100 V, giving the ions a kinetic energy of approximately 100 eV/ $z$ , where  $z$  is the number of elementary charges on the ion. The ions are analyzed in the fourth differentially pumped region that contains an orthogonal reflectron time-of-flight (TOF), used for characterizing the ions from the electrospray source. If the TOF extraction plates are grounded, the ion beam

is free to pass into a dual hemispherical deflection analyzer (HDA). Only ions having energies within a narrow range of 100 eV/z pass through the dual HDA. For experiments described here, the HDA is operated in high resolution mode, where the ions are decelerated to 10 eV/z for transmission through the HDA and then reaccelerated to 100 eV/z. With this scheme the energy resolution is 0.6% [23].

After energy selection in the HDA, ions pass into the ion trap. Initially the endcaps of the trap are set at ground and the ions can freely pass through. To initiate a trapping event, the back endcap is raised to 135 V and 0.5 ms later the front endcap is raised to 135 V. At the end of a trapping event, the endcaps are returned to ground potential in preparation for the next trapping event. Cytochrome *c* and ubiquitin ions were trapped for up to 129 ms, whereas pyruvate kinase ions were trapped for up to 391 ms. The charge detector in the center of the trap consists of a metal tube. As an ion passes through the tube, it induces a charge that is detected by a cryogenically cooled JFET (2SK152) at the input of a charge-sensitive pre-amplifier (Amptek A250). The amplified signal from the A250 is passed outside of the vacuum chamber, where it is digitized with a home-built analog-to-digital converter and stored on a computer for further offline processing.

The time-domain signals are analyzed with a program. For each trapping event, the program first does a Gaussian-apodized fast Fourier transform (FFT) on the entire event. Any peaks that rise above a predetermined noise threshold are assumed to come from ions. The noise threshold is six times the standard deviation of the noise at each frequency, plus an additional constant that is independent of frequency. This limits the number of false positives to virtually zero. The signal is not sinusoidal and we assume that any peaks above the threshold that have frequencies which are multiples of each other are from harmonics of the same ion. If there are peaks that cannot be ascribed to harmonics, they are assumed to result from multiple ions in the trap, in which case the trapping event is discarded.

This full-event FFT is useful for determining the number of ions in the trap since the frequency resolution of the FFT improves with time, but it cannot be used to determine the charge reliably. This is because the magnitude of the fundamental peak in the FFT is proportional to both the charge and the time that the ion was trapped. The trapping time cannot be determined from the full-event FFT. We often cannot see the signal from low-charge ions in the time domain, so we need another method to determine the trapping time. Our solution to this problem is to step a short, Gaussian-apodized FFT across the trapping event. Each window overlaps a portion of the previous one so that no time-domain data is skipped. To determine what width to use for this short FFT, the program begins with a 1.2 ms window. The noise is proportional to the square root of time while the ion signal is proportional to time, so the program increases the width of the window until the ion signal rises above the noise threshold. Each time this FFT window is stepped across the trapping event, the charge of the ion is measured by the magnitude of its fundamental peak,

and the  $m/z$  is determined from the frequency of the fundamental peak using the following equation:

$$\frac{m}{z} = \frac{C}{f^2} \quad (1)$$

where  $C$  is a constant (determined from SIMION simulations), which depends on both the geometry of the trap and the ion energy.

If an ion is lost from the trap, its fundamental peak disappears from the FFT. We use this signature to determine the trapping time of the ion. Once an ion is lost or the end of the trapping event is reached, the charge and  $m/z$  measurements from each window are averaged, and the resultant charge and  $m/z$  are multiplied to yield the ion's mass. The charge is calibrated by introducing test charges (ranging from approximately 1500 e to 10,000 e) through a capacitor attached to the input of the FET.

To reduce the time required to measure a spectrum, the number of single ion trapping events should be maximized. The fraction of trapping events that contain  $k$  ions is given by a Poisson distribution:

$$F(k; \lambda) = \frac{\lambda^k e^{-\lambda}}{k!} \quad (2)$$

where  $\lambda$  is the average number of ions that are trapped;  $\lambda$  is proportional to the ion current entering the trap. A plot of the probability  $F(k; \lambda)$  for no ion ( $k=0$ ), single ion ( $k=1$ ), and multiple ion ( $k>1$ ) trapping events is shown in Figure 1. According to the figure, the maximum fraction of single ion trapping events ( $k=1$ ) that can be achieved is 0.37 and this occurs when the average number of trapped ions is  $\sim 1$ . If the average number (i.e., the ion current) is reduced from this point, the fraction of empty trapping events increases, and if the average is raised, the fraction of multiple ion trapping events increases. A pair of microchannel plates located after the charge detector is used to monitor the ion current and keep it close to the optimum value.

All reagents were purchased from Sigma Aldrich (St. Louis, MO, USA). Ubiquitin (from bovine erythrocytes) was prepared at a concentration of 1 mg/mL in 1:1 water-methanol with 2% v/v acetic acid. Cytochrome *c* (equine heart) was prepared at a concentration of 2 mg/mL in 1:1 water-methanol with 2% v/v acetic acid. Pyruvate kinase (from rabbit muscle) was prepared at a concentration of 2 mg/mL in 100 mM ammonium acetate. Under the non-denaturing conditions employed here, pyruvate kinase is a tetramer. Before mass analysis, the pyruvate kinase solution was desalted using size-exclusion chromatography.

## Results

Several factors contributed to the extended trapping times achieved here. Close attention was paid to correctly aligning the ion optics, the HDA, and the ion trap. The ion optics were optimized using SIMION so that a better focused and more

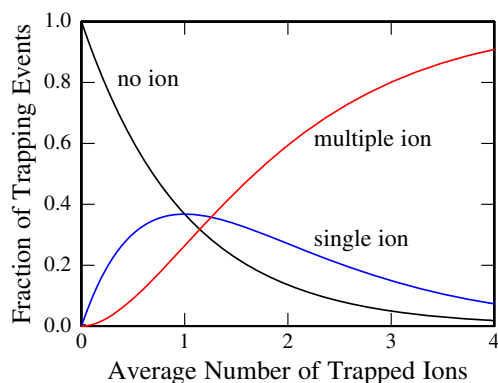


**Figure 1.** The fraction of no ion (black line), single ion (blue line), and multiple ion (red line) trapping events from a Poisson distribution (see text) plotted as a function of the average number of trapped ions

collimated ion beam enters the trap. The HDA was operated in a high resolution mode so that the ions entering the trap have a narrower energy distribution. The narrower energy distribution allows the ions to be brought to a better focus. The intensity of the ion beam was limited, so that the probability of single-ion trapping events was maximized. Finally, we have made a number of improvements to the FORTRAN program that is used to analyze the time domain signals. In particular, the program is better at identifying and excluding multiple ion trapping events (as described above).

CDMS measurements were performed for ubiquitin, cytochrome *c*, and pyruvate kinase. We chose ubiquitin because it has low charge states in its electrospray  $m/z$  spectrum. Cytochrome *c* and pyruvate kinase were chosen because they have both been characterized by CDMS before, so we are able to compare with previous results. The results for ubiquitin and cytochrome *c* show considerable overlap and so the results for cytochrome *c* are only included when they make a significant contribution to the narrative.

Cytochrome *c* and ubiquitin ions were trapped for up to 129 ms whereas pyruvate kinase ions were trapped for up to 391 ms. The distribution of trapping times is exponential with a

decay rate that depends on the ions' mass. The decay rate probably also depends on the ions' charge and their collision cross section but we have not investigated the dependence on these quantities. For ubiquitin, only around 3% of the single ion trapping events contained ions that were trapped for the full 129 ms (around 7000 cycles). On the other hand, 70% of the pyruvate kinase ions were trapped for the full 391 ms (around 6000 cycles). These observations are consistent with our experience that heavier ions have longer trapping times [24]. There are two main reasons for this. First, heavier ions have larger  $m/z$  values so they oscillate in the trap at a lower frequency and it takes longer to achieve a certain number of oscillations. In addition, heavier ions have more charge and hence more kinetic energy and so they are less strongly influenced by collisions with the background gas.

The left panel of Figure 2 shows an  $m/z$  histogram measured for ubiquitin by CDMS. Charge states ranging from +7 to +13 are clearly visible. Several ions are evident at the location expected for the +6 charge state. However, an inspection of the charges carried by these ions shows that only some of them are attributable to the +6 charge state; the others result from a dimer with a charge of +12. The  $m/z$  histogram in Figure 2 is bimodal with charge state envelopes that peak at +10 and +12. The two charge state envelopes probably result from solution phase conformations with different degrees of unfolding [33].

The right side of Figure 2 shows the mass histogram for ubiquitin, obtained by multiplying the measured  $m/z$  by the measured  $z$  for each ion. The charge determination becomes less accurate with short trapping times. For ubiquitin, only around 3% of the ions were trapped for the full 129 ms trapping period, so we included in Figure 2 all ions with trapping time greater than 40 ms (this corresponds to around 50% of the single ion trapping events). The strong peak in the mass histogram centered at around 8.5 kDa is due to ubiquitin, and the small peak around 17 kDa is due to the dimer.

It is difficult to obtain information on the detection efficiency from the experimental measurements, so we investigated this through simulations. We collected the signal with no ions in the trap (i.e., noise), added artificial signals to these noise

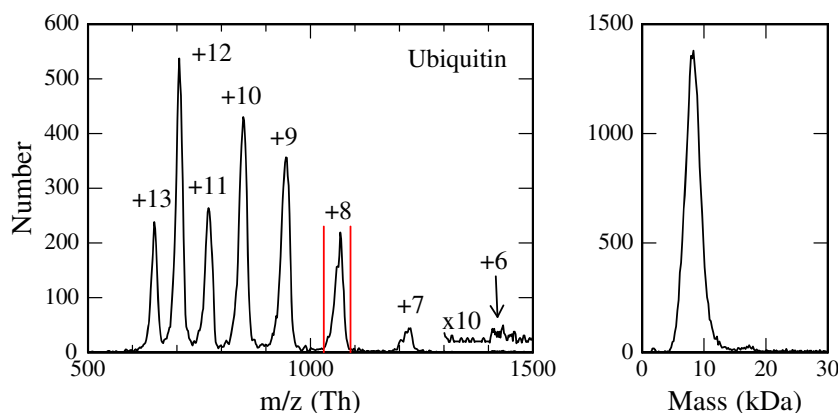


**Figure 2.** The  $m/z$  histogram (left) and  $m$  histogram (right) for ubiquitin. Results are shown for ions trapped for more than 40 ms. Charge states of +7 to +13 are seen in the  $m/z$  histogram. Peaks for the ubiquitin monomer and dimer are evident in the  $m$  histogram

files, and then analyzed them with the same program used to analyze the experimental results. The detection efficiency, or the fraction of ions detected, for a given charge state is defined as the number of simulated ions found by the analysis program divided by the number of simulated trapping events analyzed by the program. This study was performed for ubiquitin (+6 to +13), and cytochrome *c* (+8 to +19). The charge state distributions and the distributions of signal lengths used in the simulations roughly paralleled those found in the experiments. The fraction of ions detected is plotted against the charge in Figure 3. The detection efficiency is 100% for ions with nine charges and higher. For ions with fewer than nine charges, the detection efficiency decreases, reaching around 65% for the +6 charge state of ubiquitin. Only a few +6 ions were detected in the experiments (see Figure 2). However, it seems that the low abundance of the +6 charge state in the experiments is due to the low +6 signal from ubiquitin rather than due to a low detection efficiency.

To determine the accuracy of the charge measurements, the ions in the  $m/z$  histogram shown in Figure 2 were separated into their different charge states. For example, ubiquitin ions that lie between the two vertical red lines in Figure 2 can be assigned to the +8 charge state. In what follows, we refer to these ions as ions assigned to the +8 $m/z$  charge state. The mean measured charge (i.e., the mean charge measured with the charge detector) is then calculated for the ions assigned to each  $m/z$  charge state. The results of this analysis are presented in Figure 4, which shows the mean measured charge plotted against the  $m/z$  charge for ubiquitin (+7 to +13) (black squares) and cytochrome *c* (+9 to +18) (red circles). The blue line in the figure shows values where the measured image charge equals the  $m/z$  charge. The measured charge is close to the  $m/z$  charge for  $m/z$  charges greater than +14. It drops slightly below the  $m/z$  charge for intermediate values, and then rises slightly above the  $m/z$  charge for the +7. As noted above, the charge measurement is calibrated by introducing a test charge into the input of the FET through a known capacitance. The calibration is performed

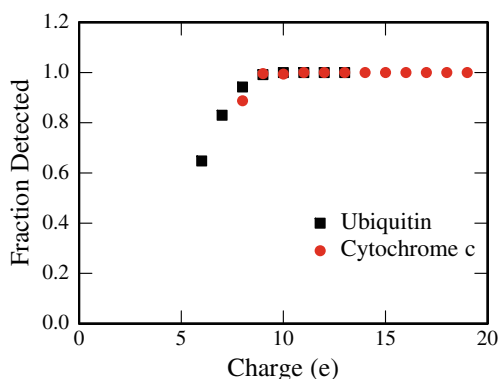


**Figure 3.** Detection efficiency determined from simulations. The fraction of ions detected is plotted against charge for ubiquitin (+6 to +13) (black squares) and cytochrome *c* (+8 to +19) (red circles). The charge state distributions and the distributions of signal lengths used in the simulations roughly paralleled those found in the experiments

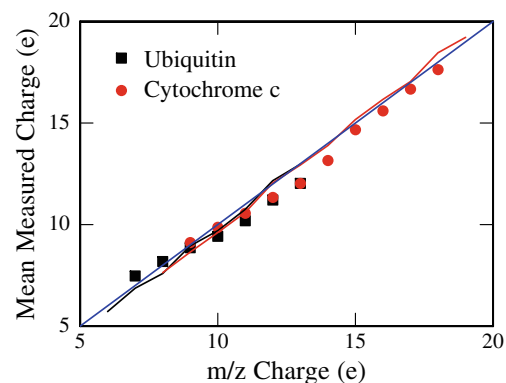


**Figure 4.** The mean charge determined from the charge measurements plotted against the  $m/z$  charge for ubiquitin (+7 to +13) (black squares) and cytochrome *c* (+9 to +18) (red circles). The black (ubiquitin) and red (cytochrome *c*) lines show the results of simulations and the blue line shows the expected behavior when the measured charge equals the  $m/z$  charge

with charges ranging from 1500 e to 10,000 e. The close agreement between the measured charges and the  $m/z$  charges for ions with 7–18 charges indicates that to a good approximation, the measured charge is directly proportional to the charge carried by the ion, at least for ions with 7 to 10,000 charges. In our previous work [24], the mean measured charges were 7%–10% larger than the  $m/z$  charges. This was attributed to a problem with the charge calibration; in the previous work, we were not able to calibrate under vacuum with a cooled JFET. In the present study, this shortcoming was addressed and the discrepancy has vanished.

The near linear relationship between the measured charge and the charge on the ion will ultimately break down for charges  $<7e$  because of noise. To prevent the data analysis program falsely identifying noise as signal, the magnitude of the peak due to the fundamental in the FFT must rise above a threshold. If the input charge is comparable to the threshold, the signals where the magnitude is enhanced by the noise are detected with higher efficiency than signals where the magnitude is reduced by the noise. As a consequence, the mean measured charge levels off at a value determined by the threshold [24]. For lower ion charges, the measured charge remains the same but the signal decreases as a smaller fraction of the signals exceed the threshold.

The black and red lines in Figure 4 show the average charges deduced from the simulations plotted against the input charge. The black and red lines closely track the blue line, indicating that the FORTRAN program used to analyze the results recovers the correct charge from the simulated data. It appears from these results that the charge is reliably measured down to six elementary charges. Although ions were detected in the experiments with a charge of 6 e, too few were found to obtain a reliable average because of the low abundance of +6 charge state from ubiquitin.

To investigate the precision of the charge measurements, the mean measured charge was subtracted from the measured charges of all ions of each  $m/z$  charge state and then the

resulting charges from all the charge states were combined and binned. The resulting histogram is shown for ubiquitin ions trapped for 129 ms (Figure 5a) and for pyruvate kinase ions trapped for 391 ms (Figure 5b). For pyruvate kinase, we have combined results for the tetramer and octamer, both of which show well-resolved charge states in the  $m/z$  histogram. In Figure 5a and b, the black line is a least squares fit of a Gaussian to the points. The RMSD obtained from the Gaussian fit is 0.95 e for ubiquitin and 0.65 e for pyruvate kinase. The RMS deviations for ubiquitin, cytochrome *c*, and pyruvate kinase ions trapped for different lengths of time were calculated in the same way. The right side of Figure 5 (panels c and d) shows the RMS deviations plotted against trapping time for ubiquitin and cytochrome *c* (c), and pyruvate kinase (d). The open points in the plot are from the simulations and the filled points are from the experimental results.

## Discussion

The blue lines in Figure 5c and d show the expected  $t^{-1/2}$  dependence of the charge RMSDs with trapping time. In both cases, the lines have been scaled to provide the best fit to the simulation results (the open points). For pyruvate kinase, the measured RMSDs (filled points) are slightly larger than the values from the simulations, and the RMSDs from both the experiments and the simulations closely track the expected  $t^{-1/2}$  dependence. There is more scatter in the results for ubiquitin

and cytochrome *c*, and the measured RMSDs are significantly larger than the values from the simulations; the differences are larger for cytochrome *c* than for ubiquitin.

One factor that probably contributes to the difference between the RMSDs from the measurements and simulations is that the peaks in the  $m/z$  spectrum are broad and it is possible that a few ions are assigned to the wrong charge state. However, the resolution in the  $m/z$  spectrum is worst for pyruvate kinase, where the measured RMSDs are closest to the values from the simulations, so this is not the only factor. The RMSDs are strongly influenced by a few outliers, and the outliers seem to be mainly responsible for difference between the RMSDs from the experiments and simulations for cytochrome *c* and ubiquitin.

With a trapping time of 391 ms the charge RMSD has been reduced to 0.65 e, which is an improvement of around a factor of two over the previous best [2]. In addition, we have reduced the limit of detection (the smallest charge that can be reliably measured) by about the same proportion, from 13 e to 7 e. The limit of detection was lowered by trapping the ions for longer and by improving the program that analyzes the time domain signals. In the early work of Benner, the limit of detection was 250 e [18]. This high limit resulted because the ions were detected on the fly and the trap was only closed when an ion was detected. In our experiment, the trap is opened and closed continuously and the results analyzed off-line to determine whether or not an ion is present. Using this approach, we are able to obtain a much lower the limit of detection. However,

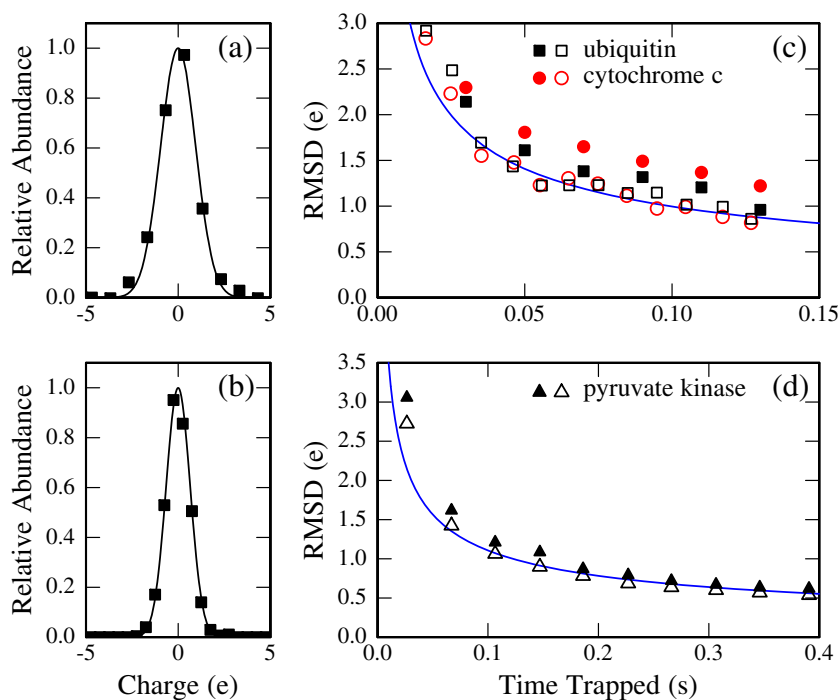


**Figure 5.** The plots on the left side show histograms of the measured charge deviation from the mean for (a) ubiquitin trapped for 129 ms and (b) pyruvate kinase ions trapped for 391 ms. The black lines show Gaussian fits to the histograms. The charge RMSDs determined from the fits are: (a) 0.95 e and (b) 0.65 e. The plots on the right side shows the charge RMSDs plotted against trapping time for: (c) ubiquitin (black squares) and cytochrome *c* (red circles); and (d) pyruvate kinase (black triangles). The filled points are the experimental data and the open points are from simulations

continuously opening and closing the trap requires larger ion currents because an ion must arrive during the short period of time when the trap is open.

The accuracy of the charge measurement factors directly into the mass resolution that can be achieved with CDMS. A detailed discussion of how the charge and  $m/z$  measurements influence the mass resolution was published previously [2]. Improving the mass resolution is of great importance in studies of mixtures of high mass ions that can result, for example, in virus assembly reactions [31]. In Figure 6, we compare the mass resolution achieved in our previous work with that obtained here. The black line shows the peak attributable to the pyruvate kinase tetramer (the native state) measured in our previous work [2], and the red line shows the same peak measured in this work. The peak measured with the longer trapping time is around 3.3 times narrower (i.e., the resolving power is around 3.3 times better than in our previous CDMS measurements for pyruvate kinase). In the previous measurements, we used a trapping time of 129 ms compared with 391 ms used here. Increasing the trapping time by a factor of three should not lead to a 3-fold reduction in the width of the peak because the RMS deviation in the charge scales as  $(\text{time})^{-1/2}$ . However, in our previous work, most of the ions were trapped for much less than 129 ms, and for the mass spectrum we included all ions trapped for more than 200 cycles (around 13 ms). With ions trapped for less than 200 cycles excluded, the average trapping time was still only 41 ms. The RMS deviation of the charge for ions included in the mass spectrum was 2.3 e, compared with 1.3 e for ions trapped for the whole 129 ms. In this work, 70% of the ions were trapped for 391 ms (around 6000 cycles) and ions that were not trapped for the full 391 ms were discarded. The RMS deviation of the charge for the ions trapped for the full 391 ms was 0.65 e. So there is a 3.5-fold reduction in the RMS deviation of the charge for ions in the mass spectra, and this is mainly responsible for the 3.3-fold improvement in the resolving power.

This work is the first time that CDMS measurements have been performed with a charge RMSD of less than 1 e. Since the

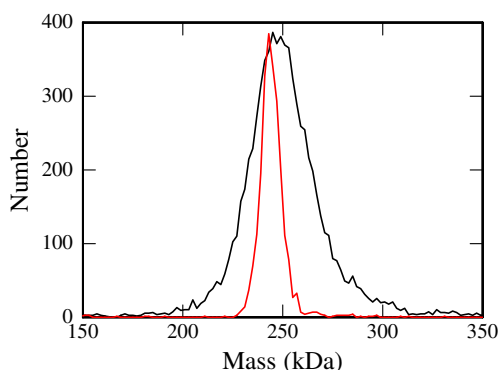


**Figure 6.** Mass histogram measured for pyruvate kinase tetramer. The black line is from our previous work (Ref. [2]). The red line is measured with the longer trapping time used in this work (391 ms) and shows the improvement in the mass resolution

charge is quantized, the goal is ultimately to define the charge state. To accomplish this with 95% confidence requires an RMSD of 0.25 e. This requires that the charge RMSD be improved by another factor of 2.6. This can be accomplished by a combination of extending the trapping time, lowering the noise, and improvements to the program used to analyze the results.

## Acknowledgments

The authors gratefully acknowledge the support of the National Science Foundation through award number 0832651. They are grateful for the technical assistance of Mr. John Pohlman and Mr. Andy Alexander in Electronic Instrument Services, and Mr. Delbert Allgood in Mechanical Instrument Services.

## References

1. Tito, M.A., Tars, K., Valegard, K., Hajdu, J., Robinson, C.V.: Electrospray time-of-flight mass spectrometry of the intact MS2 virus capsid. *J. Am. Soc. Mass Spectrom.* **122**, 3550–3551 (2000)
2. Pierson, E.E., Keifer, D.Z., Contino, N.C., Jarrold, M.F.: Probing higher order multimers of pyruvate kinase with charge detection mass spectrometry. *Int. J. Mass Spectrom.* **337**, 50–56 (2013)
3. Shelton, H., Hendricks, C.D., Wuerker, R.F.: Electrostatic acceleration of microparticles to hypervelocities. *J. Appl. Phys.* **31**, 1243–1246 (1960)
4. Hendricks, C.D.: Charged droplet experiments. *J. Colloid Sci.* **17**, 249–259 (1962)
5. Rayleigh, L.: On the equilibrium of liquid conducting masses charged with electricity. *Philos. Mag.* **14**, 184–186 (1882)
6. Keaton, P.W., Idzorek, G.C., Rowton, L.J., Seagrave, J.D., Stradling, G.L., Bergeson, S.D., Collopy, M.T., Curling, H.L., McColl, D.B., Smith, J.D.: A hypervelocity-microparticle-impacts laboratory with 100-km/s projectiles. *Int. J. Impact Eng.* **10**, 295–308 (1990)
7. Stradling, G.L., Idzorek, G.C., Shafer, B.P., Curling, H.L., Collopy, M.T., Hopkins, A.A., Fuerstenau, S.D.: Ultra-high velocity impacts: cratering studies of microscopic impacts from 3 km/s to 30 km/s. *Int. J. Impact Eng.* **14**, 719–727 (1993)
8. Chen, R., Cheng, X., Mitchell, D.W., Hofstadler, S.A., Wu, Q., Rockwood, A.L., Sherman, M.G., Smith, R.D.: Trapping, detection, and mass determination of coliphage T4 DNA ions of  $10^8$  Da by electrospray ionization Fourier transform ion cyclotron resonance mass spectrometry. *Anal. Chem.* **67**, 1159–1163 (1995)
9. Fuerstenau, S.D., Benner, W.H.: Molecular weight determination of megadalton DNA electrospray ions using charge detection time-of-flight mass spectrometry. *Rapid Commun. Mass Spectrom.* **9**, 1528–1538 (1995)
10. Schultz, J.C., Hack, C.A., Benner, W.H.: Mass determination of megadalton-DNA electrospray ions using charge detection mass spectrometry. *J. Am. Soc. Mass Spectrom.* **9**, 305–313 (1998)
11. Schultz, J.C., Hack, C.A., Benner, W.H.: Polymerase chain reaction products analyzed by charge detection mass spectrometry. *Rapid Commun. Mass Spectrom.* **13**, 15–20 (1999)
12. Fuerstenau, S.D., Benner, W.H., Thomas, J.J., Brugidou, C., Bothner, B., Siuzdak, G.: Mass spectrometry of an intact virus. *Angew. Chem. Int. Ed.* **40**, 541–544 (2001)
13. Fuerstenau, S.D.: Whole virus mass analysis by electrospray ionization. *J. Mass Spectrom. Soc. Jpn.* **51**, 50–53 (2003)
14. Doussineau, T., Kerleroux, M., Dagany, X., Clavier, C., Barbaire, M., Maurelli, J., Antoine, R., Dugourd, P.: Charging megadalton poly(ethylene oxide)s by electrospray ionization. A charge detection mass spectrometry study. *Rapid Commun. Mass Spectrom.* **25**, 617–623 (2011)
15. Doussineau, T., Bao, C.Y., Clavier, C., Dagany, X., Kerleroux, M., Antoine, R., Dugourd, P.: Infrared multiphoton dissociation tandem charge detection-mass spectrometry of single megadalton electrosprayed ions. *Rev. Sci. Instrum.* **82**, 084104 (2011)
16. Doussineau, T., Bao, C.Y., Antoine, R., Dugourd, P., Zhang, W., D'Agosto, F., Charleux, B.: Direct molar mass determination of self-assembled

- amphiphilic block copolymer nanoobjects using electrospray-charge detection mass spectrometry. *ACS Macro Lett.* **1**, 414–417 (2012)
17. Nie, Z., Cui, F., Tzeng, Y.K., Chang, H.C., Chu, M., Lin, H.C., Chen, C.H., Lin, H.H., Yu, A.L.: High-speed mass analysis of whole erythrocytes by charge-detection quadrupole ion trap mass spectrometry. *Anal. Chem.* **79**, 7401–7407 (2007)
  18. Benner, W.H.: A gated electrostatic ion trap to repetitiously measure the charge and  $m/z$  of large electrospray ions. *Anal. Chem.* **69**, 4162–4168 (1997)
  19. Gamero-Castano, M.: Induction charge detector with multiple sensing stages. *Rev. Sci. Instrum.* **78**, 043301 (2007)
  20. Gamero-Castano, M.: Retarding potential and induction charge detectors in tandem for measuring the charge and mass of nanodroplets. *Rev. Sci. Instrum.* **80**, 053301 (2009)
  21. Smith, J.W., Siegel, E.E., Maze, J.T., Jarrold, M.F.: Image charge detection mass spectrometry: pushing the envelope with sensitivity and accuracy. *Anal. Chem.* **83**, 950–956 (2011)
  22. Barney, B.L., Daly, R.T., Austin, D.E.: A multi-stage image charge detector made from printed circuit boards. *Rev. Sci. Instrum.* **84**, 114101 (2013)
  23. Contino, N.C., Jarrold, M.F.: Charge detection mass spectrometry for single ions with a limit of detection of 30 charges. *Int. J. Mass Spectrom.* **345/347**, 153–159 (2013)
  24. Contino, N.C., Pierson, E.E., Keifer, D.Z., Jarrold, M.F.: Charge detection mass spectrometry with resolved charge states. *J. Am. Soc. Mass Spectrom.* **24**, 101–108 (2013)
  25. Zilch, L.W., Maze, J.T., Smith, J.W., Ewing, G.E., Jarrold, M.F.: Charge separation in the aerodynamic breakup of micrometer-sized water droplets. *J. Phys. Chem. A* **112**, 13352–13363 (2008)
  26. Zilch, L.W., Maze, J.T., Smith, J.W., Jarrold, M.F.: Freezing, fragmentation, and charge separation in sonic sprayed water droplets. *Int. J. Mass Spectrom.* **283**, 191–199 (2009)
  27. Schmidt, H.T., Cederquist, H., Jensen, J., Fardi, A.: Conetrap: a compact electrostatic ion trap. *Nucl. Instrum. Methods B* **173**, 523–527 (2001)
  28. Zouros, T.J.M., Benis, E.P.: The hemispherical deflector analyser revisited. I. Motion in the ideal  $1/r$  potential, generalized entry conditions, Kepler orbits, and spectrometer basic equation. *J. Electron Spectrosc.* **125**, 221–248 (2002)
  29. Benis, E.P., Zouros, T.J.M.: The hemispherical deflector analyser revisited: II. Electron-optical properties. *J. Electron Spectrosc.* **163**, 28–39 (2008)
  30. Keifer, D.Z., Pierson, E.E., Bedwell, G.J., Prevelidge, P.E., Jarrold, M.F.: Charge detection mass spectrometry of bacteriophage P22 procapsid distributions above 20 MDa. *Rapid Commun. Mass Spectrom.* **28**, 483–488 (2014)
  31. Pierson, E.E., Keifer, D.Z., Selzer, L., Lee, L.S., Contino, N.C., Wang, J.C.-Y., Zlotnick, A., Jarrold, M.F.: Detection of late intermediates in virus capsid assembly by charge detection mass spectrometry. *J. Am. Chem. Soc.* **136**, 3536–3541 (2014)
  32. Kukreja, A., Wang, J.C.-Y., Pierson, E.E., Keifer, D.Z., Dragnea, B., Jarrold, M.F., Zlotnick, A.: Structurally similar woodchuck and human hepadnavirus core proteins have distinctly different temperature dependences of assembly. *J. Virol.* **88**, 14105–14115 (2014)
  33. Li, J., Taraszka, J.A., Counterman, A.E., Clemmer, D.E.: Influence of solvent composition and capillary temperature on the conformations of electrosprayed ions: unfolding of compact ubiquitin conformers from pseudonative and denatured solutions. *Int. J. Mass Spectrom.* **185/187**, 37–47 (1999)